Comparative analysis of thermoelectric elements optimum geometry between photovoltaic-thermoelectric and solar thermoelectric

Guiqiang Li*

Guiqiang.Li@hull.ac.uk

Samson Shittu

Xiaoli Ma

Xudong Zhao**

xudong.zhao@hull.ac.uk

School of Engineering, University of Hull, United Kingdom

*Corresponding author.

**Corresponding author.

Abstract

The optimization of the thermoelectric (TE) device geometry is one of the significant ways to improve its efficiency and power output. However, the complex relationship between the Photovoltaic and the thermoelectric device necessitates the need for the study of the optimum geometry of the thermoelectric device in a hybrid Photovoltaic-thermoelectric device. Therefore, this study investigates the optimum thermoelectric geometry for optimum performance of a Photovoltaic-thermoelectric (PV-TE) device and a solar thermoelectric generator (STEG). A three-dimensional finite element method is used to model the PV-TE and the STEG with different thermoelectric leg geometries. The performance of the PV-TE with two different PV cells and different TE leg geometries is investigated and compared with that of the STEG, and the optimum leg geometry for each device is identified. In addition, the effects of solar radiation and concentration ratio on the optimized device geometry performance are presented. Results obtained showed that the optimum thermoelectric geometry in a hybrid PV-TE device is dependent on the PV cell type and this is different from that of the STEG under the same conditions. The PV-TE device with cell 1 has an improved overall efficiency when a symmetrical (rectangular) thermoelectric leg is used however, this is different when the PV cell type is changed. In fact, the PV-TE device with cell 2 has an improved overall efficiency when a trapezoidal thermoelectric leg is used instead of a rectangular leg and this is the same as is the same trend observed in the case of the STEG. Therefore, the optimum geometry for a stand-alone solar thermoelectric generator cannot be directly used as a reference for the PV-TE device as the characteristics of the PV cell affects the PV-TE optimum geometry. Results from this study will indicate the different optimum geometries of STEG and PV-TE, and also provide a solid basis for optimization efforts in hybrid PV-TE devices.

Keywords: PV-TE; STEG; Trapezoidal leg; Solar irradiation; Optimum geometry

Nomenclature

A

Area, m^2

A_s

Area of SSA, m^2

C

Concentration ratio

E_{PV}

Power output of PV, W/m^2

G

Solar radiation, W/m^2

h_{rad}

Radiative heat transfer coefficient, $W/(m^2 \cdot K)$

h_{wind}

Convective heat transfer coefficient, $W/(m^2 \cdot K)$

k

Thermal conductivity, $W/(m\,K)$

L

TE Leg Height, m

P

Power output, W

Q_{flow}

Thermal energy, W

R_A

Cross-sectional area ratio of TE hot and cold junctions

R_L

Load resistance on TEG, Ω

T

Temperature, K

T_p

PV Temperature, K

T_r

Reference Temperature, K

u_w

Wind Velocity, m/s

Greek Symbols

α

Absorptivity

β_{pv}

PV temperature coefficient, K^{-1}

η

Efficiency

η_r

Reference Efficiency

η_{opt}

Optical Efficiency

Subscripts

a

Ambient

C

Cold side

H

Hot side

n

n-type

p

p-type

Abbreviations

PV

Photovoltaic

TE

Thermoelectric

SSA

Solar Selective Absorber

STEG

Solar Thermoelectric Generator

1 Introduction

The demand for electrical power is growing speedily therefore, there is an increased pressure on the existing grids to deliver this power in addition to providing a stable and sustainable supply of electricity [1,2]. In addition, the electrical energy consumption reflects the degree of economic development in a country thus, there is a relationship between economic growth and electric power consumption [3,4]. Fuel consumption and environmental pollution are two important research areas being paid more attention recently due to their direct effect on the living condition of humans [5,6]. Therefore, research on attractive green technologies for use in waste heat recovery, reducing fuel consumption in automobiles and reducing environmental pollution is urgently needed [7]. Thermoelectric generator (TEG) can convert waste heat into electricity directly without noise, pollution and moving parts based on the Seebeck effect [8–10]. It can be used in waste heat recovery in automobiles and for generating electrical power. However, the application of the thermoelectric generator is still limited due to its low conversion efficiency [11]. Nevertheless, with the thermoelectric (TE) material development, the TE demonstrates a broad potential application prospect. This is because the TE efficiency is directly related to its material by a property known as thermoelectric figure of merit. Asides material optimization, geometry optimization is another way to improve the performance of TE devices and thus increase their potential application. Therefore, the geometry design and optimization of TE, and the TE device integration application have been paid more attention to by researchers. A TE device is a solid-state device which is capable of converting waste heat into electrical energy via the Seebeck effect and it is also called a thermoelectric generator (TEG). Therefore, a solar thermoelectric generator (STEG) is simply a thermoelectric generator whose heat source is the solar irradiations from the sunlight. In reality, the STEG can be used to generate electricity thus, they are an attractive green energy solution for standalone power conversion or in hybrid solar systems. In addition, STEG have been used in power generation for health monitoring system, wireless sensors, space applications and several other low power applications. A PV-TE on the other hand is a hybrid device which combines the advantages of the Photovoltaic and thermoelectric generator. Similar to the STEG, the PV-TE can also be used to generate electricity. The overall electrical energy generation of a PV-TE is a combination of the generation from the PV and the TEG individually. In addition, the PV-TE can also be used for powering wireless sensor networks, autonomous medical devices and for terrestrial and space applications.

Sahin et al. [12] theoretically analysed the thermoelectric legs with different geometric configuration, and the results obtained indicated that the variation of the shape parameter has a favourable influence on the device efficiency. Similarly, Al-Merbati et al. [13] presented the effect of pin geometry on TE power generation and found that thermoelectric legs with trapezoidal shape enhance performance. Freunek et al. [14] built a physical model for TEG and geometric optimization was performed which resulted in the finding that Peltier heat influenced the output power of TEG by about 40%. Rezania et al. [15] optimized the TE footprint ratio, and demonstrated that the maximum output and cost-performance are achieved at $An/Ap < 1$.

Presently, the research on the Photovoltaic-thermoelectric (PV-TE) hybrid device is a growing significantly and has been paid more attention by several researchers because it can produce more electricity due to its wide solar spectrum [16–18]. Van Sark et al. [19] found that the development of new TE materials can lead to efficiency increase of about 50%. Yin et al. [20] used a theoretical analysis method to study a PV-TE system and observed an efficiency increase of about 4.6%. Shittu et al. [21] performed a parametric optimization of TE legs in PV-TE and found that the PV cell influences the PV-TE optimum geometry. Singh et al. [22] studied an irreversible concentrated PV-TE and found that Thomson effect has a negative effect on the performance of hybrid PV-TE and irreversibility increases with increase in concentration ratio. Motiei et al. [23] performed a two dimensional numerical modelling of a hybrid PV-TE device without considering Thomson effect or temperature dependent material properties. The authors observed a PV efficiency and output power enhancement of 0.59% and 5.06% respectively. Yin et al. [24] presented an optimal design method for concentrating photovoltaic-thermoelectric hybrid systems. They calculated the thermoelectric thermal resistance and presented the optimal structure of the thermoelectric generator and the effects of reference efficiency; PV temperature coefficient and thermoelectric figure of merit were studied. The authors found that the overall efficiency of the hybrid PV-TE device could be optimized by calculating the optimal temperature distribution. Babu et al. [25] presented a theoretical analysis of a novel non-concentrated flat plate hybrid PV-TE device using MATLAB/SIMULINK environment. They found that the novel system resulted in the production of 5% additional energy with an increase in the overall efficiency of 6% at standard conditions. Similarly, Lamba et al. [26] also presented a theoretical model for a hybrid PV-TE device based on first and second laws of thermodynamics and MATLAB was used to perform the numerical simulations. They found that the maximum output power and efficiency of the hybrid device increased by 5% compared to the concentrated PV only system. Li et al. analysed the primary constraint conditions for an efficient PV-TE hybrid device and found that PV-TE efficiency increases as thermoelectric leg length reduces [27,28]. Hashim et al. performed the model optimization for TE geometry in a hybrid PV- device and argued that the thermoelectric element dimension in the PV-TE has a significant influence on the overall hybrid device power output [29].

Kossyvakis et al. [30] suggested that thermoelectric devices with shorter legs should be used to obtain increased efficiency from the hybrid PV-TE device when operated under sufficient illumination. Consequently, they argued that this would allow the consumption of less material and in turn reduce the overall system cost. Kraemer et al. [31] also resonated this suggestion thus, shorter thermoelectric materials are beneficial for enhancing the performance of thermoelectric devices. In addition, Chen et al. [32] and Liu et al. [33] also performed an extensive study on the geometry optimization of thermoelectric devices however, there is limited research on the geometry optimization of thermoelectric elements in a hybrid PV-TE device. As a result of the complex relationship between the Photovoltaic and the thermoelectric device, it is imperative to find the optimum geometry for the thermoelectric device in a hybrid

PV-TE.

It can be seen from the above review that the PV-TE optimization is different from the TE alone optimization. For example, for TE alone, the aim is to maximize the TE efficiency, but for PV-TE, its total efficiency of PV and TE is a key factor for the optimization. Thus, for PV-TE device, the optimization of TE alone will not be sufficient as the PV cell performance will also influence its overall performance. That means the TE operating at its maximum conversion efficiency will not definitely lead to the maximum electrical efficiency of the PV-TE. In other words, the optimized geometry of TEG may not be suitable for PV-TE optimization.

The geometry optimization includes many aspects, such as TE length, cross-section area, and different shapes etc. At present, TE alone optimization with trapezoidal leg on the efficiency and power output can also be seen in the literatures [12,13], and this is an effective approach to increase the performance of TE alone, and may be a reference for PV-TE optimization. However, because of the different PV cells characteristics, there will be a limitation on the TEG maximum performance. Therefore, the geometry optimization results of STEG cannot be used directly in the PV-TE device as PV-TE needs to balance the PV characteristic and the TEG characteristic. Thus, for the PV-TE optimization, the trapezoidal thermoelectric leg may not be suitable for every type of PV cell it is integrated with. There are a very few researches on the best application of trapezoidal thermoelectric legs in a PV-TE for optimum performance and more so, there are only a handful of research on the comparison of PV-TE and STEG employing trapezoid leg or rectangular leg.

To make up for the above deficiency, this paper introduces two typical trapezoidal shapes for PV-TE. A finite element method is used to study the performance of the hybrid PV-TE device numerically with the aid of COMSOL Multiphysics software. The developed model is verified using published data from literature. Furthermore, the PV-TE with trapezoidal leg and rectangular leg based on two different PV cells are compared, and the PV-TE with the optimum leg geometry integrated with different PV cells is identified. In addition, the optimum thermoelectric geometry for PV-TE and STEG are also compared and the effect of solar irradiation on the optimum geometry is demonstrated. This work will present the optimum geometry for the PV-TE considering the influence of the PV cells and the thermoelectric element. Also, the optimum geometry for STEG will be presented and a comparison between the PV-TE and STEG will be made. This study will provide a valuable basis for the optimization of PV-TE considering the thermoelectric geometry for optimum performance. In addition, the results from this study will be useful to researchers interested in optimizing PV-TE and STEG.

Temperature dependent thermoelectric material properties would be used in this numerical study to avoid errors as the power output and efficiency of the thermoelectric device is affected by the temperature dependency of the thermoelectric material properties [34]. In addition, the resultant shapes (rectangular and trapezoidal) of the thermoelectric geometries studied are chosen and used in the simulations due to their ease of fabrication. In this study, the maximum output power is obtained at matched load condition (i.e. load resistance is equal to internal resistance) and finite element method is used to solve the heat transfer equations. Unlike the numerous researches reviewed above which used MATLAB/SIMULINK, this study uses COMSOL Multiphysics software which is based on the finite element method (FEM) to perform the three-dimensional numerical investigation of the STEG and PV-TE device. A major advantage of the FEM software is that, it allows the coupling of different physical models thus, Multiphysics simulations can be carried out and results can be easily visualized. Furthermore, FEM allows the performance of a detailed investigation which facilitates accurate design decision making due to its capability to allow the realization of optimization efforts. The main of this study is to investigate the optimum geometry of thermoelectric devices in stand-alone solar thermoelectric generators and in hybrid PV-TE devices. A comparative study between the performance of both devices (STEG and PV-TE) is presented and a detailed parametric study is performed to investigate the influence of geometric parameters (leg length, cross sectional area) and environmental parameters (solar radiation, concentration ratio) on the performance of STEG and PV-TE device.

The remaining part of this paper is organised as follows: Section 2 provides the geometry description and mathematical model, Section 3 provides the simulation details and model verification while Section 4 describes the results obtained and analysis of the results. Lastly, Section 5 provides the main conclusions drawn from this study.

2 Geometry description and mathematical model

The detailed description of the PV-TE and STEG investigated in this study will be presented in this section and the mathematical model used in performing the numerical simulation will also be presented.

2.1 Geometry description

For a hybrid PV-TE, the PV cell is usually attached to the TE top surface, as shown in Fig. 1(a). However, in the case of the solar thermoelectric generator (STEG), a solar selective absorber (SSA) is placed on the TE top surface instead of a PV, as shown in Fig. 1(b). The other components in both systems are: solar concentrator, tedlar, copper, cooling base, n-type and p-type legs. Tedlar is a polyvinyl fluoride film used for back surface protection in the system. Basically, it is a protective material for providing long lasting protection for devices such as PV-TE and STEG which are exposed to high temperature and harsh environmental conditions. A silicon photovoltaic cell is used together with a pair of Bismuth telluride thermoelectric elements for the hybrid PV-TE device. These same thermoelectric elements made from the same thermoelectric material are used for the STEG and temperature dependent material properties are considered in the analysis. Solar irradiation provides the external heat flux for both devices rather than a constant temperature source. A cooling base is attached to both systems to create a temperature difference in the devices and improve their electrical performance.

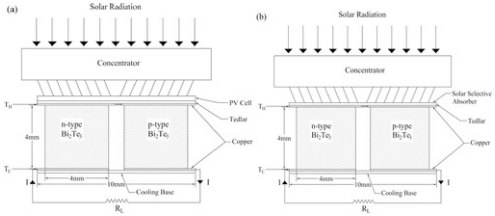

Fig. 1 Schematic diagram of (a) hybrid PV-TE and (b) STEG.

alt-text: Fig. 1

The effect of leg geometry of the TE on the performance of PV-TE and STEG was analysed. Three different leg geometry are applied to PV-TE and STEG respectively. The performance of PV-TE and STEG with the same leg geometry was compared. The cross-section area of the three-leg geometry with three different leg area ratios of $0.5,\ 1\ and\ 2$ respectively are shown in Fig. 2. As shown in Fig. 1, for both PV-TE and STEG to be analysed, the same leg geometry is used for the n-type and p-type TE legs. Different leg geometry corresponding to different leg area ratio as shown in Fig. 2 are analysed for both the PV-TE and STEG. The leg area ratio can be expressed as $R_A = A_H/A_C$. A trapezoidal leg geometry is obtained when $R_A = 0.5$ and $R_A = 2$ while a symmetrical leg geometry is obtained when $R_A = 1$. Therefore, Fig. 2(a) simply shows that A_H is half the value of A_C while the reverse is the case for Fig. 2(c).

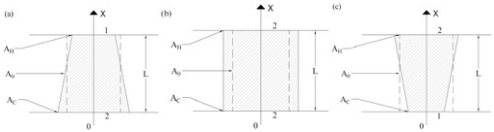

Fig. 2 Cross sectional area geometry for (a) $R_A = 0.5$, (b) $R_A = 1$ and (c) $R_A = 2$.

alt-text: Fig. 2

This research is carried out to analyse the steady-state performance of the PV-TE and STEG devices. The following assumptions are made to simplify the models:

- Heat transfer is only in one dimension.
- Uniform solar thermal distribution and temperature distribution is assumed on the surface of the PV and STEG.
- Constant room temperature of 298 K is maintained at the cold side of devices.
- All surfaces except the upper surface (hot) and lower surface(cold) are considered to be thermally insulated.
- The geometry of the p-type and n-type thermoelectric elements are identical.
- The thermoelectric elements are connected in series electrically and in parallel thermally.
- Area of the PV is the same with the area of the solar selective absorber.

2.2 Mathematical model

The mathematical equations used in numerically studying the performance of the devices are presented in this section. Three-dimensional finite element analysis is used in this study.

2.2.1 Finite element model

Finite element method is employed to solve the temperature and electric field equations in the thermoelectric unit. The coupling equations for the temperature T and electric potential V are given as [35]:

$$\nabla(k\nabla T) + \rho\mathbf{J}^2 - T\mathbf{J}\cdot\left[\left(\frac{\partial\alpha}{\partial T}\right)\nabla T + (\nabla\alpha)_T\right] = 0 \quad \textbf{(1)}$$

$$\nabla\cdot\mathbf{J} = 0 \quad \textbf{(2)}$$

$$\mathbf{J} = -\sigma\left[\nabla\left(\frac{\mu}{e} + V\right) + \alpha\nabla T\right] \quad \textbf{(3)}$$

$$q = \alpha T\mathbf{J} - k\nabla T \tag{4}$$

where k is the thermal conductivity, vector $\mathbf{J}$ is the electrical current per unit area, ρ is the electrical resistivity, σ is the electrical conductivity, α is the Seebeck coefficient, μ is the chemical potential, and e is the charge of charged particle. Considering that thermoelectric devices are not ideally one-dimensional structures, Eq. (1) shows the multidimensional effects that can be obvious in the interfaces of the modules. Furthermore, Eq. (1) and Eq. (2) form a system coupled with two partial differential equations with two dependent variables which are the temperature and electric potential. Finally, Eq. (1) can be divided into four parts reflecting the energy transferred by conduction, Joule heating, heat absorbed by Peltier effect and heat absorbed or realised by Thomson effect [35]. COMSOL Multiphysics software is used to solve all the equations above with it in built thermoelectric effect physics interface and heat transfer interface. Eq. (1) to Eq. (4) are already in built in the software therefore, they need no physical derivation.

In this research, temperature dependent thermoelectric material properties are used and they are given as [36]:

$$k_n = \left(0.0000334545 \times T^2 - 0.023350303 \times T + 5.606333\right) \ \ W/m{\cdot}K \tag{5}$$

$$k_p = \left(0.0000361558 \times T^2 - 0.026351342 \times T + 6.22162\right) \ \ W/m{\cdot}K \tag{6}$$

$$\alpha_n = \left(0.001530736 \times T^2 - 1.08058874 \times T - 28.338095\right) \times 10^{-6} \ \ V/K \tag{7}$$

$$\alpha_p = \left(-0.003638095 \times T^2 + 2.74380952 \times T - 296.214286\right) \times 10^{-6} \ \ V/K \tag{8}$$

$$\sigma_n = \left(0.01057143 \times T^2 - 10.16048 \times T + 3113.71429\right) \times 10^2 \ \ S/m \tag{9}$$

$$\sigma_p = \left(0.015601732 \times T^2 - 15.708052 \times T + 4466.38095\right) \times 10^2 \ \ S/m \tag{10}$$

where the subscript n denotes n-type thermoelectric element and p denotes p-type thermoelectric element.

The mathematical model that describes the leg geometry as shown in Fig. 2 can be written as [13]:

$$A(x) = \frac{A_H - A_C}{L}x + A_C \tag{11}$$

where $A(x)$ is the cross-sectional area of the TE legs along path x, A_C is the cross-sectional area of the leg cold side, A_H is the cross-sectional area of the leg hot side and L is the leg height. The leg area ratio is given as

$$R_A = \frac{A_H}{A_C} \tag{12}$$

Substituting Eq. (12) into Eq. (11) results in,

$$A(x) = A_0\left[1 + 2\frac{R_A - 1}{R_A + 1}\left(\frac{x}{L} - \frac{1}{2}\right)\right] \tag{13}$$

where A_0 is the cross-sectional area of the uniform leg.

Along the path x, the leg heat transfer rate can be expressed as

$$\dot{Q} = -kA(x)\frac{dT}{dx} \tag{14}$$

Assuming the heating condition is steady and the leg surfaces are isolated, Eq. (14) can be re-written as

$$\dot{Q}\int_0^L \frac{dx}{A(x)} = -k\int_{T_C}^{T_H} dT \tag{15}$$

Substituting Eq. (3) into Eq. (5) and performing integration results in,

$$\dot{Q} = \frac{2k\frac{A_0}{L}\left(\frac{R_A - 1}{R_A + 1}\right)}{\ln\left(R_A\right)}\left(T_H - T_C\right) \tag{16}$$

The overall thermal conductance of the TE leg can be expressed as

$$K_{leg} = \frac{2k\frac{A_0}{L}\left(\frac{R_A-1}{R_A+1}\right)}{\ln\left(R_A\right)} \quad (17)$$

The overall electrical resistance of the TE leg can be expressed as

$$R_{leg} = \frac{1}{2k_e\frac{A_0}{L}\left(\frac{R_A-1}{R_A+1}\right)}\ln\left(R_A\right) \quad (18)$$

2.2.2 Hybrid PV-TE model and STEG model

Two mathematical models are used to describe the performance of the hybrid PV-TE and STEG respectively.

(a) Hybrid PV-TE model

The energy balance equation in the hybrid PV-TE system can be written as [18],

$$E_{in} = E_{pv} + h_{rad}A\left(T_p - T_{sky}\right) + h_{wind}A\left(T_p - T_a\right) + Q_{flow} \quad (19)$$

where E_{in} is the solar energy absorbed by the PV-TE, E_{pv} is the electric generation of the PV, h_{rad} is the radiative heat transfer coefficient, h_{wind} is the convective heat transfer coefficient and Q_{flow} is the thermal energy transferred from the PV to the TE.

Absorbed solar energy can be written as,

$$E_{in} = CGA\alpha_c \quad (20)$$

where C is the solar concentration ratio, G is the solar irradiation, A is the PV area and α_c is the PV absorptivity.

PV electrical can be defined as [37],

$$E_{pv} = CGA\alpha_c\eta_r\left[1 - \beta_{pv}\left(T_p - T_r\right)\right] \quad (21)$$

where T_p is the PV temperature, β_{pv} is the PV temperature coefficient, η_r is the PV reference efficiency at standard conditions and T_r is the reference temperature.

h_{wind} is given as [38,39],

$$h_{wind} = 2.8 + u_w \quad (22)$$

h_{rad} is given as,

$$h_{rad} = \varepsilon\sigma\left(T_p^2 + T_{sky}^2\right)\left(T_p + T_{sky}\right) \quad (23)$$

where ε is the PV emissivity and σ is the Stefan-Boltzmann constant.

$$T_{sky} = 0.0552T_a^{1.5} \quad (24)$$

where T_a is the ambient temperature and T_{sky} is temperature of the sky.

Q_{flow} is given as,

$$Q_{flow} = Q_H \quad (25)$$

where Q_H is the energy flowing into the hot side of the TE and can be written as [40],

$$Q_H = \alpha T_H I + k\cdot T - \frac{1}{2}I^2R_{TE} \quad (26)$$

where T_H is the TE hot side temperature, I is the electrical current and R_{TE} is the internal electrical resistance.

The Q_C can be written as,

$$Q_C = \alpha T_C I + k \cdot T + I^2 R_{TE} \quad (27)$$

The power output of the TEG is given as,

$$P_{TE} = I^2 R_L \quad (28)$$

where R_L is the load resistance.

The efficiency of the TEG is given as,

$$\eta_{TE} = \frac{P_{TE}}{Q_H} \quad (29)$$

Therefore, the overall efficiency of the PV-TE can be written as follow,

$$\eta_{PV-TE} = \frac{E_{pv} + P_{TE}}{CGA} \quad (30)$$

(b) STEG model

The input solar energy absorbed at the surface of the STEG can be expressed as [41],

$$Q_{in} = CGA_s \alpha_s \eta_{opt} \quad (31)$$

where A_s is the area of SSA (placed on surface of STEG), α_s is the STEG absorptivity and η_{opt} is the optical efficiency which is assumed to be 100%.

Similar to the PV-TE model described above, the radiative and convective heat losses are also considered in the STEG model and the equations are the same.

$$Q_{rad} = h_{rad} A_s \left(T_p - T_{sky}\right) \quad (32)$$

$$Q_{cov} = h_{wind} A_s \left(T_p - T_a\right) \quad (33)$$

The efficiency of the TEG has been given in Eq. (29). Therefore, the overall efficiency of the STEG can be given as [42]:

$$\eta_{STEG} = \eta_{TE} \alpha_{cs} \eta_{opt} \quad (34)$$

3 Simulation and verification

3.1 Simulation details

COMSOL 5.3 Multiphysics commercial software is used to simulate the PV-TE and the STEG. In this research, two different types of PV cells are used to study the performance of the hybrid PV-TE. For Cell 1, reference efficiency of 10% is used and its temperature coefficient value is 0.001/K; while for Cell 2, reference efficiency of 15% is used and temperature coefficient value is 0.004/K Simulation parameters used for both the PV cells are shown in Table 1. Temperature dependent material properties are used for the thermoelectric elements as described in Eq. (5) - Eq. (10); while constant material properties obtained from COMSOL material library are used for Silicon, Tedlar, Copper and Alumina which are the other system components. The cross-sectional area of the SSA and that of the PV is assumed to be the equivalent to the cross-sectional area of the thermoelectric module.

Table 1 Simulation parameters.

alt-text: Table 1

Parameters	Symbol	Value	References
SSA area	A_s	0.0001m²	
PV area	A	0.0001m²	[27]

PV thickness	Th_{PV}	0.0003 m	[43]
Tedlar thickness	Th_{ted}	0.000175 m	[43]
Copper thickness	Th_{co}	0.0001m^2	[44]
TE area	A_{TE}	0.000016m^2	
TE height	L	0.004 m	
SSA absorptivity	α_s	0.93	[45]
PV absorptivity	α_c	0.9	[43]
SSA emissivity	ε_s	0.8	[45]
PV emissivity	ε	0.8	[44]
Ambient temperature	T_a	298 K	[46]
Solar irradiation	G	1000 W/m^2	[46]
Concentration ratio	c	4	
Wind velocity	u_w	1 m/s	[44]
Cell 1 reference efficiency (STC)	η_r	10%	[29]
Cell 1 temperature coefficient	β_{pv}	0.001K^{-1}	[29]
Cell 2 reference efficiency (STC)	η_r	15%	[47]
Cell 2 temperature coefficient	β_{pv}	0.004K^{-1}	[47]
Reference temperature	T_r	298 K	[29]

3.2 Model validation

The above model was validated using published data in Ref. [38], the simulation was carried out using our model under the same conditions as those in Ref. [38]. Temperature dependent material properties used in the study were incorporated and the results are presented in Figs. 3 and 4. Furthermore, Fig. 3 shows the comparison of the TEG efficiency results obtained from the previous study and this present study while Fig. 4 shows the comparison of the TEG power output between the two studies. It is clear from Figs. 3 and 4 that the results obtained in both studies are in good agreement thus, the model used in this present study is validated. In addition, it can be seen from Fig. 4 that there exists an optimum leg height for obtaining maximum output power from the TE device. This is the reason for the sharp point (maximum output power) and beyond this optimum leg height, the TE output power is reduced.

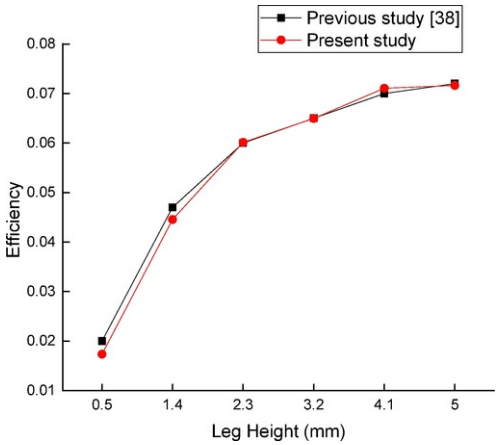

Fig. 3 TEG efficiency validation of previous study with present simulation.

alt-text: Fig. 3

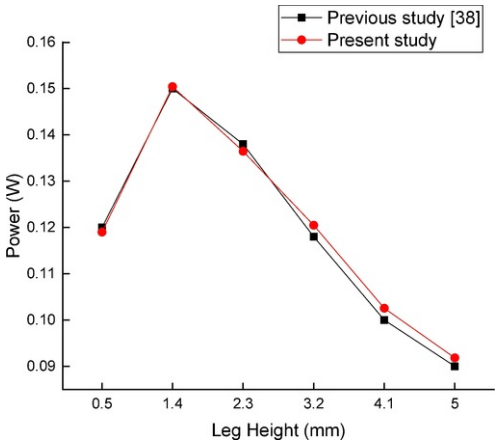

Fig. 4 TEG power validation of previous study with present simulation.

alt-text: Fig. 4

4 Results and discussion

In this section, the results obtained from the numerical study are presented and a detailed comparison between the PV-TE and STEG is provided under different conditions. Furthermore, the effects of solar radiation and concentration ratio on the performance of both devices (STEG and PV-TE) are discussed.

4.1 Detailed comparison of PV-TE and STEG

The two PV-TE with different leg geometry using Cell 1 and Cell 2 respectively and the STEG are all simulated using very similar parameters so as to compare the results obtained from the different systems. The three systems are analysed for the leg area ratio $R_A = 0.5,\ 1\ and\ 2$. The mesh diagrams of the PV-TE and STEG with different leg geometry are shown in Fig. 5.

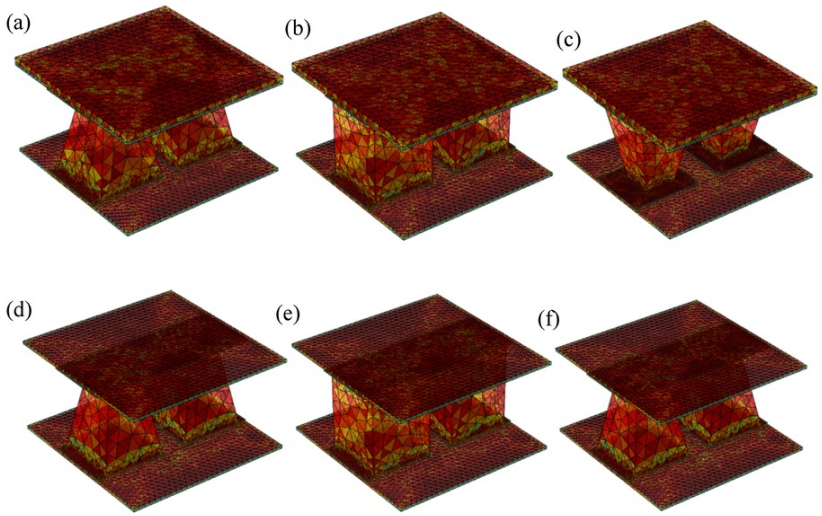

Fig. 5 Mesh diagrams of the PV-TE with trapezoidal and rectangular legs (a) $R_A = 0.5$, (b) $R_A = 1$, (c) $R_A = 2$ and the STEG (d) $R_A = 0.5$, (e) $R_A = 1$, (f) $R_A = 2$.

alt-text: Fig. 5

4.1.1 Comparison for the condition of $R_A = 0.5$

When $R_A = 0.5$ (trapezoidal leg), the variation of TE leg height and area with the overall efficiency of each of the three systems is shown in Figs. 6–8 respectively. With the increase of TE leg height, the overall PV-TE efficiency decreases. From Fig. 6, it can be seen that when the TE leg area is 16 mm^2 and PV cell 1 is used, the PV-TE efficiency is the lowest compared to all other TE leg area at that particular leg height. However, this efficiency increases gradually as the leg height increases and finally decreases. This shows that there is an optimum leg area and leg height at which the maximum PV-TE efficiency can be obtained. Considering Fig. 7, it can be observed that the efficiency of the PV-TE for all leg area considered decrease as the leg height increases. This trend is different from that of Fig. 6, because of the difference in the characteristics of the PV cells used.

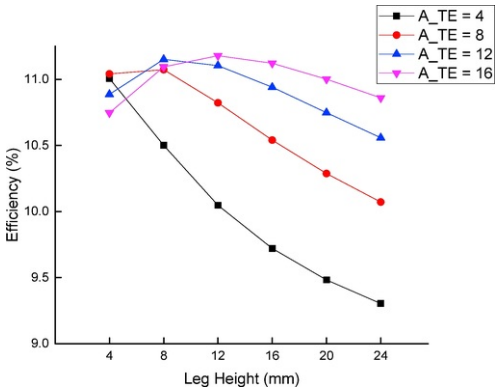

Fig. 6 Variation of overall efficiency of PV-TE with TE height and area increase using Cell 1, $R_A = 0.5$.

alt-text: Fig. 6

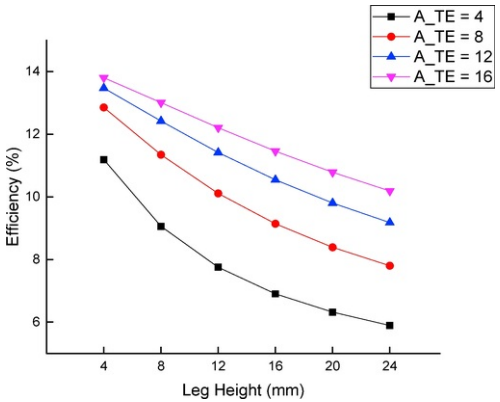

Fig. 7 Variation of overall efficiency of PV-TE with TE height and area increase using Cell 2, $R_A = 0.5$.

alt-text: Fig. 7

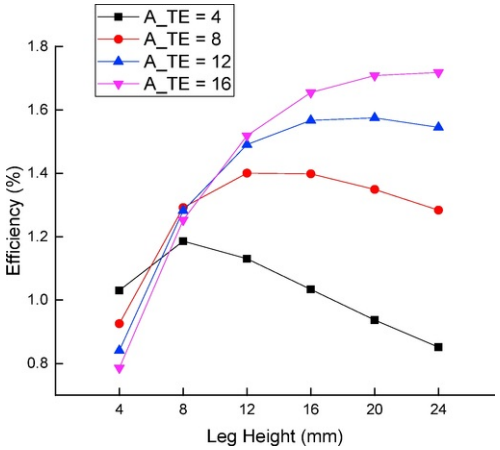

Fig. 8 Variation of STEG efficiency with TE height and area increase, $R_A = 0.5$.

alt-text: Fig. 8

For a STEG, the overall system efficiency firstly increases then decreases as the TE leg height increases (Fig. 8). Similar to the tendency of the PV-TE using PV cell 1, when leg area is 16 mm^2, the efficiency of STEG is also initially lower then higher than those with the smaller leg area. However, the maximum efficiency of the PV-TE with cell 1 and cell 2 can be obtained at different thermoelectric geometry as is the case of the STEG. The highest efficiency of the PV-TE using cell 1 is obtained when the leg height is 12 mm, while that of the PV-TE using cell 2 is obtained when the leg height is 4 mm. The highest efficiency of the STEG occurs at the leg height of 24 mm. All these variation in optimum geometry reemphasises the need for this study and more optimization study to be performed so that the optimum geometry can be used for each of the devices. In addition, Fig. 8 clearly shows that for the particular leg area ratio being considered ($R_A = 0.5$) there exists an optimum leg height and area at which the STEG is most efficient. This is the reason for the graph trend observed as the efficiency firstly increases as the leg height increased for the different leg areas till it reaches an optimum point at which no further efficiency increase can be achieved thus, it starts decreasing.

The TE output power for each of the three devices considered in this study (PV-TE using cell 1, PV-TE using cell 2 and STEG) when the leg area ratio $R_A = 0.5$ is shown in Fig. 9. It can be seen that there exists an optimum leg height at which maximum output power can be obtained from each of the devices and this optimum leg height is different for each device. This is because for the PV-TE, the PV efficiency is enhanced at low temperature values however the reverse is the case for the TEG efficiency thus, the efficient integration of both devices requires the optimization of hybrid system as a whole. In addition, different PV temperature coefficient values used would affect the temperature of the TE hot side while the absence of PV and presence of SSA in the STEG would also cause the hot side temperature to be different. Consequently, there will be a different temperature difference in each system and the resulting TE output power will be different.

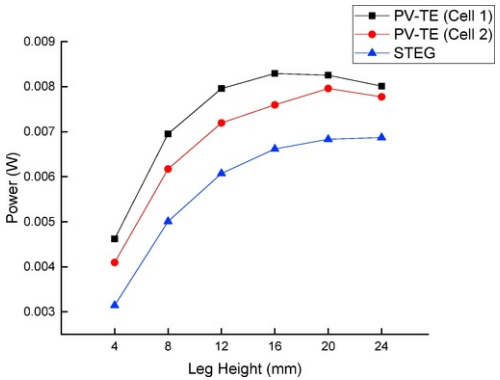

Fig. 9 TE output power in PV-TE Cell 1, PV-TE Cell 2 and STEG, $R_A = 0.5$.

alt-text: Fig. 9

4.1.2 Comparison for the condition of $R_A = 1$

When $R_A = 1$ (rectangular leg), the variations of the PV-TE and STEG overall efficiency with TE leg height for different leg area are presented in Figs. 10–12. In this condition, the tendency of the efficiency curve for PV-TE with cell 2 is similar with that of PV-TE with cell 1. However, when $R_A = 1$, the optimal leg heights are 8 mm, 12 mm, 16 mm and 24 mm for the leg areas of 4 mm^2, 8 mm^2, 12 mm^2, 16 mm^2 respectively, and these are different from the optimum leg and area of the PV-TE with cell 1 (Fig. 10). In addition, the advantage of PV-TE with the leg area of 16 mm^2 is not clear in most cases. However, when the TE is integrated with PV cell 2, the variation tendency of the overall efficiency with the increase of the leg height at different leg areas are the same as that with PV cell 1 (Fig. 11).

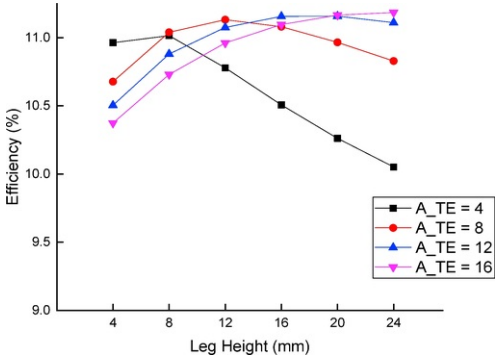

Fig. 10 Variation of overall efficiency of PV-TE with TE height and area increase using Cell 1, $R_A = 1$.

alt-text: Fig. 10

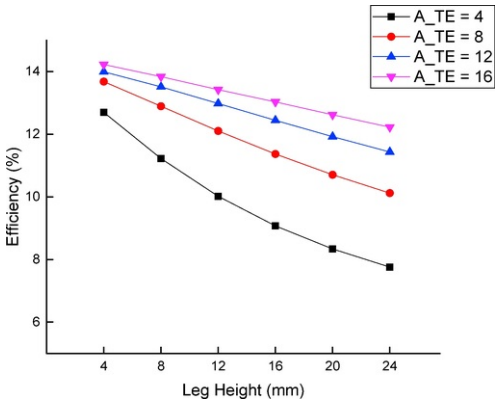

Fig. 11 Variation of overall efficiency of PV-TE with TE height and area increase using Cell 2, $R_A = 1$.

alt-text: Fig. 11

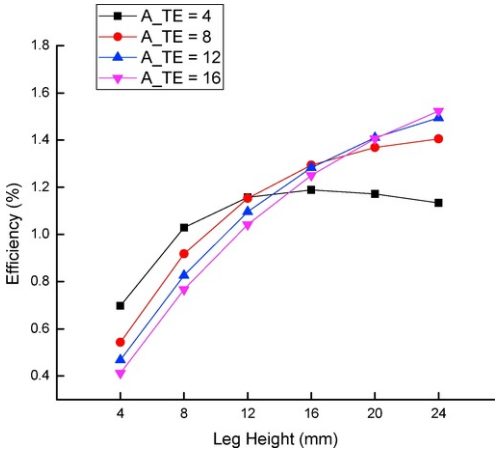

Fig. 12 Variation of STEG efficiency with TE height and area increase, $R_A = 1$.

alt-text: Fig. 12

When $R_A = 1$, the advantage of the STEG with the leg area of 16 mm^2 is not obvious. In the leg height scope of 4 mm–12 mm, the smaller leg area may be better (Fig. 12). In addition, it can also be seen that the optimum leg height will increase with the leg area rising. The variation of the TE output power in the different PV-TE and STEG is presented in Fig. 13 and it can be seen that with the increase of leg height, the outputs all show a rising trend.

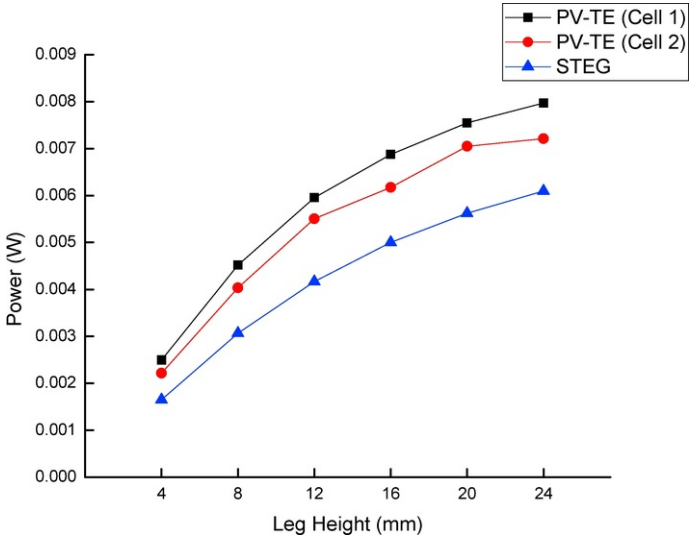

Fig. 13 TE output power in PV-TE Cell 1, PV-TE Cell 2 and STEG, $R_A = 1$.

alt-text: Fig. 13

4.1.3 Comparison for the condition of $R_A = 2$

When $R_A = 2$ (inverted trapezoid leg), the geometry of the trapezoidal leg is obtained by a 180° rotation of the geometry when $R_A = 0.5$. Therefore, the variations of TE leg height and area with the overall efficiency and the output power are very identical to the results with $R_A = 0.5$.

4.2 Overall efficiency comparison

Different leg area ratios will result in different optimum geometry condition for obtaining maximum efficiency from the PV-TE and STEG. Fig. 14 shows the variation of overall system efficiency with TE leg area ratios for 4 mm^2 leg height and 16 mm^2 leg area for each system considered. It can be seen from Fig. 14 that the optimum TE geometry in the hybrid PV-TE using Cell 1 is the same with that of the STEG and this geometry is asymmetrical. However, the optimum TE geometry in the hybrid PV-TE using Cell 2 is different (it is symmetrical). In addition, it is clear from the values obtained that $R_A = 2$ is the optimum geometry for the PV-TE system using Cell 1 and the STEG while $R_A = 1$ is the optimum geometry for the PV-TE system using Cell 2.

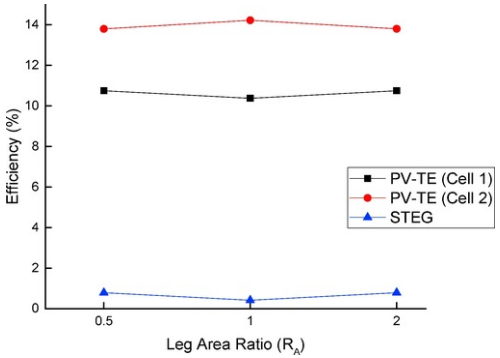

Fig. 14 Overall efficiency variation with leg area ratio.

alt-text: Fig. 14

4.3 Effect of solar radiation on optimum geometry

From Figs. 14 and 6, it is clear that the optimized geometry and parameter for the PV-TE using Cell 1 is $R_A = 2$, TE leg height 12 mm and TE leg area 16 mm^2. The variation of the overall efficiency with the solar concentration ratio using this optimized geometry is shown in Fig. 15. It can be seen clearly that the overall efficiency increases as solar radiation increases. From Figs. 14 and 11, it can be observed that the optimized geometry and parameter for the PV-TE using Cell 2 is $R_A = 1$, TE leg height 4 mm^2 and TE leg area 16 mm^2. The resulting effect of solar radiation on this optimized geometry can be observed in Fig. 16. It is obvious from Fig. 16 that the overall efficiency decreases as the solar radiation increases. This is different from the trend shown in Fig. 15 and this difference is caused by the difference in cell used. Furthermore, from Figs. 14 and 8, it is clear that the optimized geometry and parameter for the STEG is $R_A = 2$, TE leg height 24 mm^2 and TE leg area 16 mm^2. The variation of the overall efficiency of STEG with solar concentration ratio is shown in Fig. 17. It can be seen that the overall efficiency also increases as solar radiation increases and this is similar to the trend observed in Fig. 15.

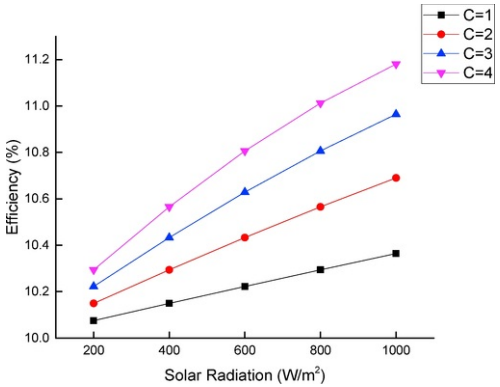

Fig. 15 Variation of overall efficiency of PV-TE using Cell 1 with solar radiation increase.

alt-text: Fig. 15

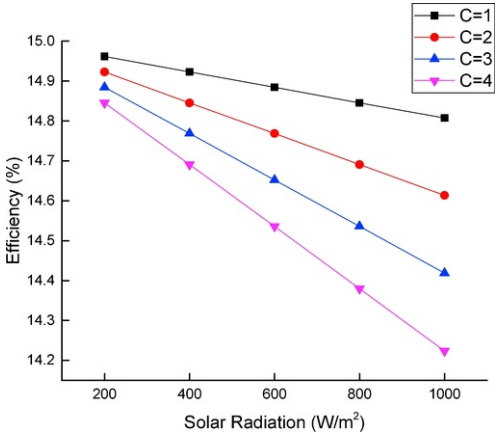

Fig. 16 Variation of overall efficiency of PV-TE using Cell 2 with solar radiation increase.

alt-text: Fig. 16

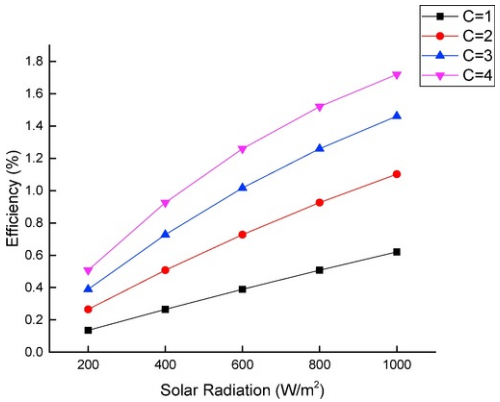

Fig. 17 Variation of STEG efficiency with solar radiation increase.

alt-text: Fig. 17

5 Conclusion

In this study, the utilization of different thermoelectric leg geometry for the enhancement of PV-TE and STEG performance has been investigated. Three different leg area ratios ($R_A = 0.5,\ 1\ and\ 2$) resulting in trapezoidal, rectangular and inverted trapezoidal leg geometries respectively were used to study the performance of two PV-TE devices using two different cells and a STEG device. The effects of the PV cell characteristics on the performance of the PV-TE in relation to the different leg geometries were presented. A three-dimensional finite element model was developed and verified before being used to study the performance of the devices numerically. COMSOL 5.3 Multiphysics software was employed to perform the numerical simulations and the comparison between PV-TE with different PV cells and STEG was demonstrated. In addition, the effect of solar irradiation on the optimum PV-TE and STEG geometry was analysed.

As a result of the different PV cells characteristics, the performance results of the PV-TE devices were in contrast. PV-TE with cell 1 had a higher overall efficiency when the symmetrical (rectangular) thermoelectric leg was used in comparison with the trapezoidal legs. However, when the TEG was integrated with PV cell 2, the PV-TE with the trapezoidal leg had a higher efficiency compared to the one with the rectangular leg and this trend was also observed in the STEG. Therefore, the optimum results for STEG cannot be used as a reference for the PV-TE directly as the PV cell characteristics need to be considered.

In addition, the PV with a high temperature coefficient can be matched with the TE of large leg area and low height. However, the PV-TE with a low PV temperature coefficient has a complex trend similar to that of the STEG. Furthermore, solar radiation will also have different effects on the different PV-TE and STEG. Therefore, for PV-TE optimization, the trapezoidal leg is not suitable for all PV-TE as the PV cell characteristics need to be considered. The main conclusions from this study can therefore be summarized as;

1. The optimum thermoelectric geometry in a hybrid PV-TE device using Cell 1 is the same with that of the STEG and this geometry is obtained when $R_A = 2$ (inverted trapezoid leg).
2. In contrast, the optimum thermoelectric geometry in a hybrid PV-TE device using Cell 2 is symmetrical $R_A = 1$ (rectangular leg).
3. The optimization results for a stand-alone STEG cannot be directly referenced by the PV-TE device due to the influence of the PV cell characteristics on the overall performance.
4. The overall efficiency of the PV-TE using Cell 1 and the STEG increased as the solar radiation increased however, a reverse trend was observed for the PV-TE using Cell 2. This was as a result of the different characteristics of the PV cell used in each device.

Acknowledgment

This study was sponsored by the Project of EU Marie Curie International incoming Fellowships Program (745614). The authors would also like to express our appreciation for the financial supports from EPSRC (EP/R004684/1) and Innovate UK (TSB 70507–481546) for the Newton Fund - China-UK Research and Innovation Bridges Competition 2015 Project ‘A High Efficiency, Low Cost and Building Integrate-able Solar Photovoltaic/Thermal (PV/T) system for Space Heating, Hot Water and Power Supply’ and DongGuan Innovation Research Team Program (No. 2014607101008).

References

[1] S.H.A. Kaboli, A. Fallahpour, J. Selvaraj and N.A. Rahim, Long-term electrical energy consumption formulating and forecasting via optimized gene expression programming, *Energy* **126**, 2017, 144–164, https://doi.org/10.1016/j.energy.2017.03.009.

[2] M. Modiri-Delshad, S.H. Aghay Kaboli, E. Taslimi-Renani and N.A. Rahim, Backtracking search algorithm for solving economic dispatch problems with valve-point effects and multiple fuel options, *Energy* **116**, 2016, 637–649, https://doi.org/10.1016/j.energy.2016.09.140.

[3] S.H.A. Kaboli, J. Selvaraj and N.A. Rahim, Long-term electric energy consumption forecasting via artificial cooperative search algorithm, *Energy* **115**, 2016, 857–871, https://doi.org/10.1016/j.energy.2016.09.015.

[4] S.H.A. Kaboli, A. Fallahpour, N. Kazemi, J. Selvaraj and N.A. Rahim, An expression-driven approach for long-term electric power consumption forecasting, *Am J Data Min Knowl Discov* **1**, 2016, 16–28, https://doi.org/10.11648/j.ajdmkd.20160101.13.

[5] M. Rahimi-Gorji, M. Ghajar, A.H. Kakaee and D. Domiri Ganji, Modeling of the air conditions effects on the power and fuel consumption of the SI engine using neural networks and regression, *J Braz Soc Mech Sci Eng* **39** 2017, 375–384, https://doi.org/10.1007/s40430-016-0539-1.

[6] N. Ahmed, N. Ali Shah, B. Ahmad, S.I.A. Shah, S. Ulhaq and M.R. Gorji, Transient MHD convective flow of fractional nanofluid between vertical plates, *J Appl Comput Mech* 2018, https://doi.org/10.22055/jacm.2018.26947.1364.

[7] T.M.O. Diallo, M. Yu, J. Zhou, X. Zhao, S. Shittu, G. Li, et al., Energy performance analysis of a novel solar PVT loop heat pipe employing a microchannel heat pipe evaporator and a PCM triple heat exchanger, *Energy* **167**, 2019, 866–888 https://doi.org/10.1016/j.energy.2018.10.192.

[8] G. Li, J. Ji, G. Zhang, W. He, X. Chen and H. Chen, Performance analysis on a novel micro-channel heat pipe evacuated tube solar collector-incorporated thermoelectric generation, *Int J Energy Res* **40**, 2016, 2117–2127, https://doi.org/10.1002/er.3589.

[9] G. Li, W. Feng, Y. Jin, X. Chen and J. Ji, Discussion on the solar concentrating thermoelectric generation using micro-channel heat pipe array, *Heat Mass Tran* **53**, 2017, 3249–3256, https://doi.org/10.1007/s00231-017-2026-3.

[10] G. Li, S. Shittu, T.M.O. Diallo, M. Yu, X. Zhao and J. Ji, A review of solar photovoltaic-thermoelectric hybrid system for electricity generation, *Energy* **158**, 2018, 41–58, https://doi.org/10.1016/j.energy.2018.06.021.

[11] W. He, G. Zhang, X. Zhang, J. Ji, G. Li and X. Zhao, Recent development and application of thermoelectric generator and cooler, *Appl Energy* **143**, 2015, 1–25 https://doi.org/10.1016/j.apenergy.2014.12.075.

[12] A.Z. Sahin and B.S. Yilbas, The thermoelement as thermoelectric power generator: effect of leg geometry on the efficiency and power generation, *Energy Convers Manag* **65**, 2013, 26–32, https://doi.org/10.1016/j.enconman.2012.07.020.

[13] A.S. Al-Merbati, B.S. Yilbas and A.Z. Sahin, Thermodynamics and thermal stress analysis of thermoelectric power generator: influence of pin geometry on device performance, *Appl Therm Eng* **50**, 2013, 683–692, https://doi.org/10.1016/j.applthermaleng.2012.07.021.

[14] M. Freunek, M. Müller, T. Ungan, W. Walker and L.M. Reindl, New physical model for thermoelectric generators, *J Electron Mater* **38**, 2009, 1214–1220, https://doi.org/10.1007/s11664-009-0665-y.

[15] A. Rezania, L.A. Rosendahl and H. Yin, Parametric optimization of thermoelectric elements footprint for maximum power generation, *J Power Sources* **255**, 2014, 151–156, https://doi.org/10.1016/j.jpowsour.2014.01.002.

[16] X. Ju, Z. Wang, G. Flamant, P. Li and W. Zhao, Numerical analysis and optimization of a spectrum splitting concentration photovoltaic-thermoelectric hybrid system, *Sol Energy* **86**, 2012, 1941–1954, https://doi.org/10.1016/j.solener.2012.02.024.

[17] G. Li, X. Zhao and J. Ji, Conceptual development of a novel photovoltaic-thermoelectric system and preliminary economic analysis, *Energy Convers Manag* **126**, 2016, 935–943, https://doi.org/10.1016/j.enconman.2016.08.074.

[18] G. Li, K. Zhou, Z. Song, X. Zhao and J. Ji, Inconsistent phenomenon of thermoelectric load resistance for photovoltaic–thermoelectric module, *Energy Convers Manag* **161**, 2018, 155–161, https://doi.org/10.1016/j.enconman.2018.01.079.

[19] W.G.J.H.M. Van Sark, Feasibility of photovoltaic - thermoelectric hybrid modules, *Appl Energy* **88**, 2011, 2785–2790, https://doi.org/10.1016/j.apenergy.2011.02.008.

[20] E. Yin, Q. Li and Y. Xuan, One-day performance evaluation of photovoltaic-thermoelectric hybrid system, *Energy* **143**, 2018, 337–346, https://doi.org/10.1016/j.energy.2017.11.011.

[21] S. Shittu, G. Li, X. Zhao and X. Ma, Series of detail comparison and optimization of thermoelectric element geometry considering the PV effect, *Renew Energy* 2018, https://doi.org/10.1016/j.renene.2018.07.002.

[22] S. Singh, O.I. Ibeagwu and R. Lamba, Thermodynamic evaluation of irreversibility and optimum performance of a concentrated PV-TEG cogenerated hybrid system, *Sol Energy* **170**, 2018, 896–905, https://doi.org/10.1016/j.solener.2018.06.034.

[23] P. Motiei, M. Yaghoubi, E. GoshtashbiRad and A. Vadiee, Two-dimensional unsteady state performance analysis of a hybrid photovoltaic-thermoelectric generator, *Renew Energy* **119**, 2018, 551–565, https://doi.org/10.1016/j.renene.2017.11.092.

[24] E. Yin, Q. Li and Y. Xuan, Optimal design method for concentrating photovoltaic-thermoelectric hybrid system, *Appl Energy* **226**, 2018, 320–329, https://doi.org/10.1016/j.apenergy.2018.05.127.

[25] C. Babu and P. Ponnambalam, The theoretical performance evaluation of hybrid PV-TEG system, *Energy Convers Manag* **173**, 2018, 450–460, https://doi.org/10.1016/j.enconman.2018.07.104.

[26] R. Lamba and S.C. Kaushik, Solar driven concentrated photovoltaic-thermoelectric hybrid system: numerical analysis and optimization, *Energy Convers Manag* **170**, 2018, 34–49, https://doi.org/10.1016/j.enconman.2018.05.048.

[27] G. Li, X. Chen and Y. Jin, Analysis of the primary constraint conditions of an efficient photovoltaic-thermoelectric hybrid system, *Energies* **10**, 2017, 1–12, https://doi.org/10.3390/en10010020.

[28] G. Li, X. Zhao, Y. Jin, X. Chen, J. Ji and S. Shittu, Performance analysis and discussion on the thermoelectric element footprint for PV–TE maximum power generation, *J Electron Mater* **47**, 2018, 5344–5351, https://doi.org/10.1007/s11664-018-6421-4.

[29] H. Hashim, J.J. Bomphrey and G. Min, Model for geometry optimisation of thermoelectric devices in a hybrid PV/TE system, *Renew Energy* **87**, 2016, 458–463, https://doi.org/10.1016/j.renene.2015.10.029.

[30] D.N. Kossyvakis, G.D. Voutsinas and E.V. Hristoforou, Experimental analysis and performance evaluation of a tandem photovoltaic-thermoelectric hybrid system, *Energy Convers Manag* **117**, 2016, 490–500, https://doi.org/10.1016/j.enconman.2016.03.023.

[31] D. Kraemer, K. McEnaney, M. Chiesa and G. Chen, Modeling and optimization of solar thermoelectric generators for terrestrial applications, *Sol Energy* **86**, 2012, 1338–1350, https://doi.org/10.1016/j.solener.2012.01.025.

[32] W.H. Chen, C.C. Wang, C.I. Hung, C.C. Yang and R.C. Juang, Modeling and simulation for the design of thermal-concentrated solar thermoelectric generator, *Energy* **64**, 2014, 287–297, https://doi.org/10.1016/j.energy.2013.10.073.

[33] Z. Liu, S. Zhu, Y. Ge, F. Shan, L. Zeng and W. Liu, Geometry optimization of two-stage thermoelectric generators using simplified conjugate-gradient method, *Appl Energy* **190**, 2017, 540–552, https://doi.org/10.1016/j.apenergy.2017.01.002.

[34] F. Meng, L. Chen and F. Sun, Effects of temperature dependence of thermoelectric properties on the power and efficiency of a multielement thermoelectric generator, *Int J Energy Environ* **3**, 2012, 137–150.

[35] Y. Wu, T. Ming, X. Li, T. Pan, K. Peng and X. Luo, Numerical simulations on the temperature gradient and thermal stress of a thermoelectric power generator, *Energy Convers Manag* **88**, 2014, 915–927, https://doi.org/10.1016/j.enconman.2014.08.069.

[36] European Thermodynamics Limited, GM250-127-14-16 Thermoelectric generator module - Datasheet, 2014, 1–4.

[37] G. Li, G. Pei, J. Ji, M. Yang, Y. Su and N. Xu, Numerical and experimental study on a PV/T system with static miniature solar concentrator, *Sol Energy* **120**, 2015, 565–574 https://doi.org/10.1016/j.solener.2015.07.046.

[38] J.-L. Gao, Q.-G. Du, X.-D. Zhang and X.-Q. Jiang, Thermal stress analysis and structure parameter selection for a Bi2Te3-based thermoelectric module, *J Electron Mater* **40**, 2011, 884–888,

https://doi.org/10.1007/s11664-011-1611-3.

[39] J.H. E. a. Wattmuff, Solar and wind induced external coefficient for solar collectors, *Coop Mediterr Pour I'Energue Solaire, Rev Int d'Heliotechnique* 1977, 56–60, 2nd Quart.

[40] W. He, G. Zhang, G. Li and J. Ji, Analysis and discussion on the impact of non-uniform input heat flux on thermoelectric generator array, *Energy Convers Manag* **98**, 2015, 268–274 https://doi.org/10.1016/j.enconman.2015.04.006.

[41] P. Li, L. Cai, P. Zhai, X. Tang, Q. Zhang and M. Niino, Design of a concentration solar thermoelectric generator, *J Electron Mater* **39**, 2010, 1522–1530, https://doi.org/10.1007/s11664-010-1279-0.

[42] J. Xiao, T. Yang, P. Li, P. Zhai and Q. Zhang, Thermal design and management for performance optimization of solar thermoelectric generator, *Appl Energy* **93**, 2012, 33–38, https://doi.org/10.1016/j.apenergy.2011.06.006.

[43] R. Lamba and S.C. Kaushik, Modeling and performance analysis of a concentrated photovoltaic-thermoelectric hybrid power generation system, *Energy Convers Manag* **115**, 2016, 288–298, https://doi.org/10.1016/j.enconman.2016.02.061.

[44] G. Li, X. Chen, Y. Jin and J. Ji, Optimizing on thermoelectric elements footprint of the photovoltaic-thermoelectric for maximum power generation, *Energy Procedia* **142**, 2017, 730–735, https://doi.org/10.1016/j.egypro.2017.12.119.

[45] G. Li, G. Zhang, W. He, J. Ji, S. Lv, X. Chen, et al., Performance analysis on a solar concentrating thermoelectric generator using the micro-channel heat pipe array, *Energy Convers Manag* **112**, 2016, 191–198, https://doi.org/10.1016/j.enconman.2016.01.025.

[46] Y.Y. Wu, S.Y. Wu and L. Xiao, Performance analysis of photovoltaic-thermoelectric hybrid system with and without glass cover, *Energy Convers Manag* **93**, 2015, 151–159, https://doi.org/10.1016/j.enconman.2015.01.013.

[47] G. Li, G. Pei, J. Ji and Y. Su, Outdoor overall performance of a novel air-gap-lens-walled compound parabolic concentrator (ALCPC) incorporated with photovoltaic/thermal system, *Appl Energy* **144**, 2015, 214–223 https://doi.org/10.1016/j.apenergy.2015.01.112.

Highlights

- Optimum geometry for thermoelectric in Photovoltaic-thermoelectric was presented.
- Comparison of solar thermoelectric device and Photovoltaic-thermoelectric was done.
- Three-dimensional numerical simulation using finite element method was presented.
- Two Photovoltaic cells with different thermoelectric geometries were analysed.

Queries and Answers

Query: Please confirm that the provided emails "Guiqiang.Li@hull.ac.uk, xudong.zhao@hull.ac.uk" are the correct address for official communication, else provide an alternate e-mail address to replace the existing one, because private e-mail addresses should not be used in articles as the address for communication.
Answer: Yes.

Query: Please check whether the order of designated corresponding authors is correct, and amend if necessary.
Answer: Yes.

Query: Have we correctly interpreted the following funding source(s) and country names you cited in your article: EPSRC, United Kingdom; Innovate UK, United Kingdom; Newton Fund, United Kingdom?
Answer: Yes

Query: Please confirm that given names and surnames have been identified correctly and are presented in the desired order and please carefully verify the spelling of all authors' names.
Answer: Yes

Query: Your article is registered as belonging to the Special Issue/Collection entitled "Energy EU China". If this is NOT correct and your article is a regular item or belongs to a different Special Issue please contact s.venkiteswaran@elsevier.com immediately prior to returning your corrections.
Answer: Yes